V European Conference on Computational Fluid Dynamics
ECCOMAS CFD 2010
J. C. F. Pereira and A. Sequeira (Eds)
Lisbon, Portugal, 14–17 June 2010

IMPROVEMENTS OF SIMPLE LOW-DISSIPATION AUSM AGAINST SHOCK INSTABILITIES IN CONSIDERATION OF INTERFACIAL SPEED OF SOUND

Keiichi Kitamura* **and Eiji Shima***

* Japan Aerospace Exploration Agency (JAXA)
Sagamihara, Kanagawa 252-5210, Japan
e-mail: kitamura.keiichi@jaxa.jp, shima.eiji@jaxa.jp

Key words: Numerical Flux, Shock Instability, Carbuncle Phenomenon, AUSM-Family, Interfacial Speed of Sound, SLAU

Abstract. *Numerical experiments for hypersonic flows using AUSM-family flux functions have been conducted in one-dimensional (1D) and multi-dimensional (1.5D) contexts. We paid a particular attention to "interfacial speed of sound $c_{1/2}$ (i.e., speed of sound numerically defined at cell-interface)," and its definition has been proved to improve robustness of AUSM-family fluxes against shock anomalies, i.e., both shock instabilities and oscillations. This finding motivated us further to investigate the behaviour of our recently proposed scheme, SLAU (Simple Low-dissipation AUSM). Finally, we reached the present modification in which numerical dissipation term in pressure flux function was changed to be proportional to interfacial Mach number at supersonic speeds. The improved scheme, named SLAU2, showed universal robustness against the shock anomalies irrelevant to $c_{1/2}$. SLAU2 is considered to be "properly dissipative" for both shock and contact discontinuities, and also for low speed flow computations.*

1 INTRODUCTION

Hypersonic flow computations still suffer from anomalous solutions such as a "carbuncle phenomenon[1, 2, 3, 4] (Fig.1)." It is very easy from simple examples in Fig.1 to find a "correct" solution. However, in practical simulations involving complex geometries with complex flow phenomena (Ref. [5], for instance), it is almost impossible to identify such anomalies, if any. This difficulty degrades the reliability of currently available CFD methods and afflicts the use of them in hypersonic flows.

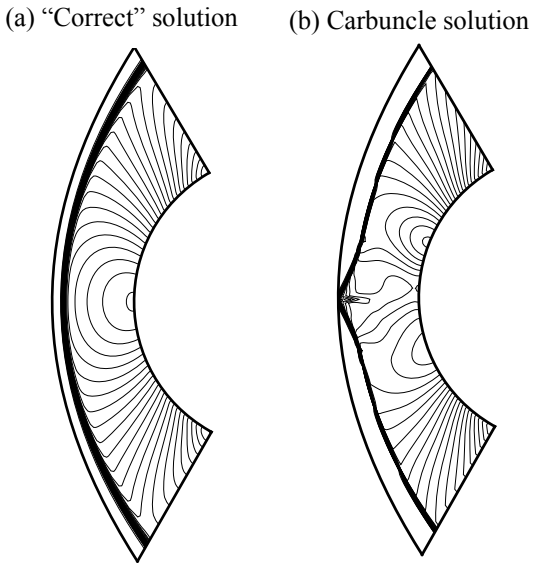

Fig. 1 2-D blunt-body simulation results.

Those anomalies are sometimes called "shock instabilities,[6,7]" because they occur at numerically resolved shock waves by finite-volume, shock-capturing methods.[2] Usage of those terminologies are scattered even among the related-researchers, and a part of the reasons lies in the fact that it is still an open question whether the carbuncle phenomenon is numerical artifact or not. Until almost a decade ago, the carbuncle had been regarded as a numerical anomalous solution[2]; however, more recent studies[8, 9, 10, 11] argued that the carbuncle was a rather mathematical or physical solution. In the present study, we take the viewpoint that the shock anomalies are partly caused by the lack of mathematical expression for internal shock structure by the governing equations[12] on the grounds that

- The carbuncle appears as one of the physical solutions, as if a spike is mounted ahead of a blunt-body in a hypersonic flow.[13] This fact excludes the following simple classification: A physical solution is "correct," and a carbuncle solution is unphysical.
- In the real physics, a shock wave has finite thickness and inside structure. From the viewpoint of continuum mechanics, on the other hand, a shock wave is regarded as a zero-thickness discontinuity. Euler equations to be solved are based on the latter, but a numerically captured shock (by shock-capturing methods) usually contains a few computational cells forming numerical internal shock structure.[14, 15, 16]
- The numerical shock structure violates Euler equations and/or the Rankine-Hugoniot relation.[14, 15] Both are valid only "across" the shock, not "inside" it. Further discussions are found in Refs. [4, 6, 16, 17].
- There is no reported anomalous solution by a shock-fitting method which produces no shock width.[2, 18]

Then, among the scattered terminologies, we redefined the shock related anomalous solutions* as in Table1[12], that is, "shock anomalies" are categorized into two phenomena of "shock oscillations" and "shock instabilities." The carbuncle belongs to the latter family and appears only in multi-dimensions. "Oscillations" stand for the oscillatory behaviors of the captured shock, whether in time or space, confined within only two cells. Such situations often arise when, in a non-shock-aligned grid, the shock jumps

* Although the conventional term "shock instabilities" is used in the title of the present paper, we will use the new, recently updated definitions of "shock anomalies (Table 1)" in the rest of the paper.

from one set of mesh line to another.[12] The spatially multi-dimensional oscillation is also referred to as "asymmetry."

We now clearly see that the shock anomalies should not have any single cause, nor is there any single cure.[4] It is difficult to establish such cures theoretically, because we still have not reached an accepted conclusions for how numerical internal shock structure should be expressed, as stated above. It is also difficult to establish them experimentally, because the anomalies depend on mesh geometry, mesh size, flow Mach number, and specific heat ratio.[2,4,12] Nevertheless, Kitamura et al.[4] conducted experimental investigations by paying particular attention to "flux functions" and "mesh." In their numerical experiments, one dimensional and multi-dimensional shock anomalies are independently tested for many flux functions.

Anomalies	Oscillations	Instabilities
1D	Y (in time)[†]	N (Not observed yet)
Multi-D	Y (both in time and space)	Y (Carbuncle)

Table 1 Shock anomalies

Thus, in this work, SLAU (Simple Low-dissipation AUSM) flux recently developed by the authors[19] is tested first as the same manner as Refs. [4, 12]. The SLAU is one of low-dissipation schemes of AUSM-family, but free from any tunable parameters. SLAU showed an excellent performance at low speeds,[19, 20] not to mention in moderate speed regimes, but as many other flux functions, anomalous behaviors were observed at shocks under some circumstances.

In the present paper, after brief explanations for the computational methods (Sec. 2), fundamental discriptions for "cell-interfacial speed of sound," denoted as $c_{1/2}$, will be given (Sec. 3). The $c_{1/2}$ is the speed of sound numerically defined at a cell-interface, usually, and used to calculate an AUSM-family numerical flux.[19, 21, 22] We will focus on the role of $c_{1/2}$, and the numerical tests in Refs. [4, 12] (reviewed in Sec. 4) will be conducted for SLAU and other fluxes (Sec. 5).

The definition of $c_{1/2}$ is included in the above-mentioned question of what the numerical shock structure should be, since $c_{1/2}$ is left as a scheme's parameter while other physical quantities at the cell-interfaces such as primitive variables are somehow interpolated from cell-center values. Naturally, the $c_{1/2}$ has many options, and it will be explored in the present work which expression is suitable for SLAU or other AUSM-family fluxes for improvements of its robustness/stability against the captured shocks.

Ref. [23] is, to the best of the authors' knowledge, the only one in which the effects of $c_{1/2}$ was studied for high Mach numbers. Liou and Edwards[23] revealed that slight modifications of $c_{1/2}$ can influence stability of the shock for AUSM+ and even Roe flux[24] or Van Leer's FVS.[25] However, their discussions were limited to one dimension and the most of their work was dedicated to low speed flow discussions. As demonstrated in Ref. [4], 1D and multi-dimensional shock anomalies should be considered separately, and this will be done in the present work.

Finally, based on the findings in Sec. 5, the SLAU flux will be modified to have more proper amount of dissipation both inside and outside the shock (Sec. 6). As will be demonstrated from numerical examples, the improved scheme, named SLAU2, is promising for a broad spectrum of flow speed regimes.

[†] The authors used the term "1D carbuncle" in the earlier work[4], but here we abandoned this expression to avoid confusions.

2 COMPUTATIONAL METHOD

2.1 Governing Equations

The governing equations are the two-dimensional, compressible Euler or Navier-Stokes equations:

$$\frac{\partial \mathbf{Q}}{\partial t}+\frac{\partial \mathbf{E}}{\partial x}+\frac{\partial \mathbf{F}}{\partial y}=0 \quad \text{: Euler} \tag{1a}$$

$$\frac{\partial \mathbf{Q}}{\partial t}+\frac{\partial \mathbf{E}}{\partial x}+\frac{\partial \mathbf{F}}{\partial y}=\frac{\partial \mathbf{E}_v}{\partial x}+\frac{\partial \mathbf{F}_v}{\partial y} \quad \text{: Navier-Stokes} \tag{1b}$$

$$\mathbf{Q}=\begin{bmatrix}\rho\\ \rho u\\ \rho v\\ \rho E\end{bmatrix},\quad \mathbf{E}=\begin{bmatrix}\rho u\\ \rho u^2+p\\ \rho uv\\ \rho uH\end{bmatrix},\quad \mathbf{F}=\begin{bmatrix}\rho v\\ \rho vu\\ \rho v^2+p\\ \rho vH\end{bmatrix},\quad \mathbf{E}_v=\begin{bmatrix}0\\ \tau_{11}\\ \tau_{21}\\ u_j\tau_{jk}+\kappa\dfrac{\partial T}{\partial x}\end{bmatrix},\quad \mathbf{F}_v=\begin{bmatrix}0\\ \tau_{12}\\ \tau_{22}\\ u_j\tau_{jk}+\kappa\dfrac{\partial T}{\partial y}\end{bmatrix} \tag{2}$$

$$\tau_{jk}=\mu\left[\left(\frac{\partial u_j}{\partial x_k}+\frac{\partial u_k}{\partial x_j}\right)-\frac{2}{3}\frac{\partial u_l}{\partial x_l}\delta_{jk}\right] \tag{3}$$

where ρ is density, u, v are velocity components in Cartesian coordinates, E is total energy, p is pressure, H is total enthalpy [$H = E + (p/\rho)$], and T is temperature. The working gas is assumed to be air approximated by the calorically-perfect-gas model with the specific heat ratio γ =1.4. The Prandtl number is Pr=0.72. The molecular viscosity μ is calculated by the Sutherland's formula, and the thermal conductivity κ is given by $\kappa = \mu c_p/\mathrm{Pr}$, where c_p is specific heat at constant pressure.

2.2 Computational Method

The following methods are used for computations herein, if not mentioned otherwise.

As for spatial discretization, the primitive variables at cell centers are used also as cell-interfacial values for spatially first order cases; In second order simulations, the primitive variables at each cell-interface are interpolated by using MUSCL reconstruction[26] with Van Albada's limiter.[27] Then, inviscid fluxes at the cell-interface are calculated from the following flux functions:

SLAU:

$$\mathbf{F}_{1/2}=\frac{\dot{m}+|\dot{m}|}{2}\mathbf{\Psi}^{+}+\frac{\dot{m}-|\dot{m}|}{2}\mathbf{\Psi}^{-}+\tilde{p}\mathbf{N} \tag{4a}$$

$$\mathbf{\Psi}=(1,\,u,\,v,\,H)^T,\qquad \mathbf{N}=(0,\,n_x,\,n_y,\,0)^T \tag{4b}$$

Mass flux:

$$\dot{m}=\frac{1}{2}\left\{\rho_L\left(V_{nL}+|\overline{V}_n|^{+}\right)+\rho_L\left(V_{nL}-|\overline{V}_n|^{-}\right)-\frac{\chi}{c_{1/2}}\Delta p\right\} \tag{4c}$$

$$|\overline{V}_n|=\frac{\rho_L|V_{nL}|+\rho_R|V_{nR}|}{\rho_L+\rho_R} \tag{4d}$$

$$|\overline{V}_n|^+ = (1-g)|\overline{V}_n| + g|V_{nL}|, \qquad (4e)$$
$$|\overline{V}_n|^- = (1-g)|\overline{V}_n| + g|V_{nR}|$$

$$g = -\max\left[\min\left(M_L, 0\right), -1\right] \cdot \min\left[\max\left(M_R, 0\right), 1\right] \quad \in [0, 1] \qquad (4f)$$

Pressure flux:

$$\tilde{p} = \frac{p_L + p_R}{2} + \frac{f_{pL}^+\big|_{\alpha=0} - f_{pR}^-\big|_{\alpha=0}}{2}\left(p_L - p_R\right) + \left(1-\chi\right)\left(f_{pL}^+\big|_{\alpha=0} + f_{pR}^-\big|_{\alpha=0} - 1\right)\frac{p_L + p_R}{2} \qquad (4g)$$

$$\chi = (1-\widehat{M})^2 \qquad (4h)$$

$$\widehat{M} = \min\left(1.0, \frac{1}{c_{1/2}}\sqrt{\frac{u_L^{\,2} + v_L^{\,2} + u_R^{\,2} + v_R^{\,2}}{2}}\right) \qquad (4i)$$

where the <u>interfacial speed of sound</u> $c_{1/2}$ is given by

$$c_{1/2} = \overline{c} = 0.5\left(c_L + c_R\right) \qquad (4j)$$

and

$$f_p^{\pm}\big|_{\alpha} = \begin{cases} \frac{1}{2}\left(1 \pm sign(M)\right), & if\ |M| \geq 1 \\ \frac{1}{4}\left(M \pm 1\right)^2\left(2 \mp M\right) \pm \alpha M\left(M^2 - 1\right)^2, & otherwise \end{cases} \qquad (4k)$$

$$M = \frac{V_n}{c_{1/2}} = \frac{un_x + vn_y}{c_{1/2}} \qquad (4l)$$

<u>AUSM+</u>:

$$\mathbf{F}_{1/2} = \frac{\dot{m} + |\dot{m}|}{2}\mathbf{\Psi}^+ + \frac{\dot{m} - |\dot{m}|}{2}\mathbf{\Psi}^- + \tilde{p}\mathbf{N} \qquad (5a)$$

$$\mathbf{\Psi} = \left(1, u, v, H\right)^T, \qquad (5b)$$
$$\mathbf{N} = \left(0, n_x, n_y, 0\right)^T$$

Mass flux:

$$\dot{m} = M_{1/2}c_{1/2}\begin{cases} \rho_L & if\ M_{1/2} > 0 \\ \rho_R & otherwise \end{cases} \qquad (5c)$$

$$M_{1/2} = f_{ML}^+\big|_{\beta=1/8} + f_{MR}^-\big|_{\beta=1/8} \qquad (5d)$$

Pressure flux:

(5e)

$$\tilde{p} = f_{p_L}^{+}\Big|_{\alpha=3/16} p_L + f_{p_R}^{-}\Big|_{\alpha=3/16} p_R$$

and the <u>interfacial speed of sound</u> $c_{1/2}$ is

$$c_{1/2} = \min(\tilde{c}_L, \tilde{c}_R), \quad \tilde{c} = c^{*2}/\max(c^*, |V_n|) \tag{5f}$$

where

$$c^{*2} = \frac{2(\gamma-1)}{(\gamma+1)} H \tag{5g}$$

is critical speed of sound, and

$$f_M^{\pm}\Big|_\beta = \begin{cases} \frac{1}{2}(M \pm |M|), & if\ |M| \geq 1 \\ \pm\frac{1}{4}(M \pm 1)^2 \pm \beta(M^2-1)^2, & otherwise \end{cases} \tag{5h}$$

Viscous fluxes are computed by using second order central difference in viscous simulations, whereas for time integration, forward Euler method (first order in time), or LU-SGS is employed.

3 INTERFACIAL SPEED OF SOUND

Most of AUSM-family schemes, including all-speed schemes such as AUSM$^+$-up,[22] LDFSS,[28] LSHUS,[29] SLAU,[19] and SD-SLAU,[30] need speed of sound at the cell interface. A simple arithmetic averaging in Eq. (4j), for example, works well for LSHUS, SLAU and SD-SLAU for general cases.

On the other hand, another definition in Eq. (5f) is used for AUSM+ to capture normal shock properly. Other choices are also possible for AUSM+, such as

$$c_{1/2} = \max(\tilde{c}_L, \tilde{c}_R), \quad \tilde{c} = c^{*2}/\max(c^*, |V_n|) \tag{6a}$$

or geometric average,

$$c_{1/2} = \sqrt{c_L c_R} \tag{6b}$$

All of these definitions and even Roe-average,

$$c_{1/2} = \hat{c} = \sqrt{(\gamma-1)(\hat{H} - 0.5\hat{q}^2)}, \quad \hat{q}^2 = \hat{u}^2 + \hat{v}^2 \tag{6c}$$

are applicable to above-mentioned AUSM-family schemes.

The choice of the interface sound of speed $c_{1/2}$ has little effect on low or moderate Mach number flows (M<1), obviously because c_L and c_R are exactly or almost equal to each other. However, as will be shown later, it has significant influence on numerical stability/robustness of the schemes at a shock at higher Mach numbers. Ref. [23] is, to the best of the authors' knowledge, the only one in which the effects of $c_{1/2}$ was studied for high Mach number flows. Liou and Edwards[23] revealed that slight modifications of $c_{1/2}$ in Eq.(5f) to the form of Eq.(6a) generally stabilized the shock for AUSM+ and

even Roe flux or Van Leer's FVS. However, their discussions were limited to one dimension and the most of their work was dedicated to low speed flow discussions. As demonstrated in Ref. [4], 1D and multi-dimensional shock anomalies should be considered separately, and this will be done later in the present work.

Figure 2 shows an example of how $c_{1/2}$ differs depending on its definitions for a Mach 6 normal shock. The abscissa stands for index of the cell-interface, and the ordinate the cell-interfacial speed of sound, $c_{1/2}$, standardized by the freestream velocity, U_∞. The normal shock is placed exactly at the cell-interface between i=12 and 13 cells (= 12th interface) in the 50 cells of a one-dimensional computational grid (shown later in Fig. 3). Then, the $c_{1/2}$ is extracted at the very beginning of the computation (before the temporal evolution in the first timestep)[‡] for each definition.

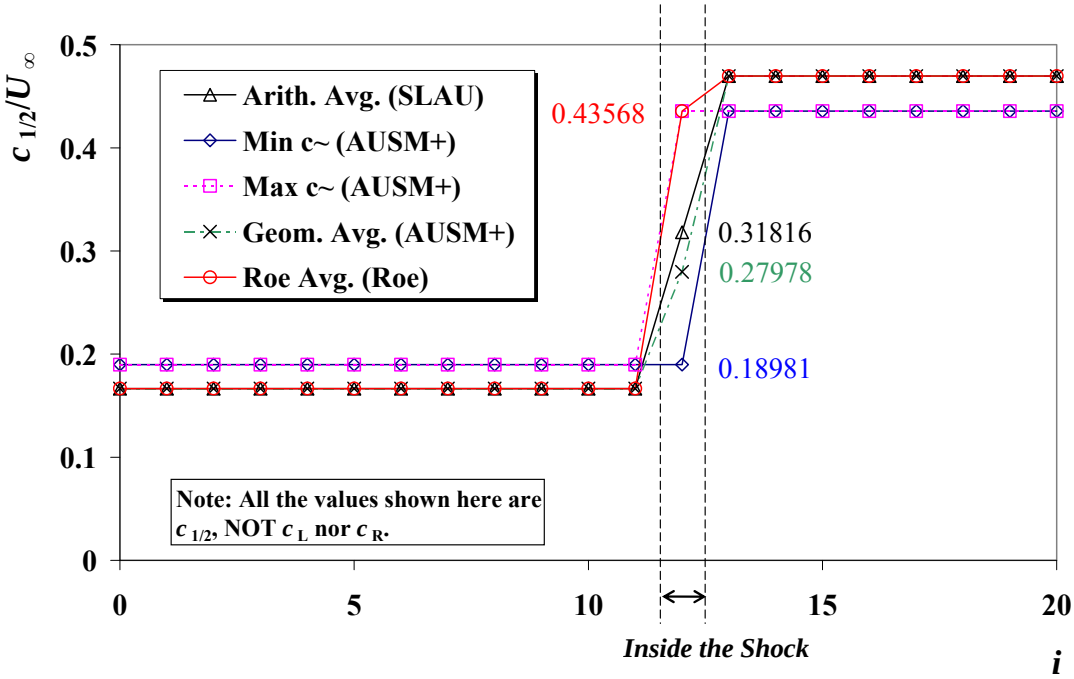

Fig. 2 Interfacial speed of sound $c_{1/2}$ (standardized by freestream Mach number, 6.0) with different definitions for normal shock.

It is seen from the graph that the interfacial speed of sound, $c_{1/2}$, changes dramatically "inside" the shock, while it is uniform elsewhere. The arithmetic averaged value from Eq. (4j), 0.31816, is in the middle of the five definitions, and the Eq. (5f), AUSM+ default, gave 0.18981 which is approximately 60% of the arithmetic averaged value. This difference will increase with Mach number (e.g, at a stronger shock), because the sound speeds c_L and c_R will differ more between both sides of the discontinuity. Note that the interface speed of sound $c_{1/2}$ controls the amount of numerical diffusion in some of the numerical flux function (the third term of Eq. (4g), for instance). Effects of changing these definitions on the shock stability/robustness of the schemes will be examined in the next section.

We remind the readers of that this modification of $c_{1/2}$ is only applicable to internal shock; the speed of sound "outside" the shock is retained.

[‡] Thus, any of numerical methods in the code, such as flux functions, affected the calculated values of $c_{1/2}$. Hand-calculations also yielded the same outputs.

4 NUMERICAL EXPERIMENTS

4.1 1D (One-Dimensional) Steady Normal Shock Test

From the viewpoint of continuum mechanics, a shock wave is regarded as a thin jump discontinuity, but a captured shock has numerical internal structure. However, it is hard to establish what this internal structure should be.[14, 15, 16] For example, the Godunov and Roe schemes produce an intermediate state that lies on the Hugoniot curve joining $\mathbf{Q}_R$ to $\mathbf{Q}_L$, but such a state does not preserve mass flux inside the shock.[14] On the other hand, at least one intermediate state is needed to allow representation of a shock that is not precisely located at a mesh interface. Even more, as already shown in Fig. 2, the shock precisely lying on the cell interface has its internal structure having a degree of freedom for choice of the sound speed $c_{1/2}$. Therefore, following Ref. [4], we will first conduct the "1D test" in order to see the role of $c_{1/2}$ for AUSM-family schemes on the shock stability/robustness.

In this test, we prescribe initial conditions that include an intermediate state and boundary conditions that force the shock to remain in its initial position. The grid comprises 50 equally spaced cells, as in Fig. 3, with initial conditions for left (L: $i \le 12$) and right (R: $i \ge 14$):

$$\mathbf{Q}_L = \begin{bmatrix} 1 \\ 1 \\ 0 \\ \dfrac{1}{\gamma(\gamma-1)M_\infty^2} + \dfrac{1}{2} \end{bmatrix}, \quad \mathbf{Q}_R = \begin{bmatrix} f(M_\infty) \\ 1 \\ 0 \\ \dfrac{g(M_\infty)}{\gamma(\gamma-1)M_\infty^2} + \dfrac{1}{2f(M_\infty)} \end{bmatrix} \tag{7a}$$

where

$$f(M_\infty) = \left(\frac{2}{(\gamma+1)M_\infty^2} + \frac{\gamma-1}{\gamma+1} \right)^{-1}, \quad g(M_\infty) = \frac{2\gamma M_\infty^2}{\gamma+1} - \frac{\gamma-1}{\gamma+1} \tag{7b}$$

following the Rankine-Hugoniot conditions across the normal shock. The internal shock conditions (M: i=13) are as follows:

1) The density is given as

$$\rho_M = \varepsilon \rho_L + (1-\varepsilon)\rho_R \tag{7c}$$

where the shock-position parameter $\varepsilon = 0.0, 0.1, \ldots, 0.9$.

2) The other variables are calculated based on ρ_M so that all variables lie on the Hugoniot curve, connected to $\mathbf{Q}_L$ and $\mathbf{Q}_R$, as in Ref. [16].

At the outflow boundary we prescribe the mass flux at the ghost cell ($i = i_{\max}+1$):

$$(\rho u)_{i\max+1,\, j} = (\rho u)_\infty = 1 \tag{7d}$$

for the mass in the whole computational domain to remain constant and for the shock to be fixed at the same position; meanwhile, other values are simply extrapolated (e.g., $\rho_{i\max+1,j} = \rho_{i\max,j}$).

The inflow boundary has the freestream values. The freestream Mach number was chosen in the range $1.5 \leq M_\infty \leq 20.0$ in the original paper[4]; however, here only M_∞=6.0 is chosen because the solutions in the 1-D problem were almost the same for $M_\infty \geq 6.0$ in Ref. [4]. Then, the computations are first order both in spatial and temporal accuracy, and conducted until 40,000 steps with CFL=0.5. If a scheme is always stable for all the values of ε, the scheme can be labeled as 1-D stable. Typical solutions are shown in Fig. 4 in which a stable solution is labeled as '2: Good,' and an oscillatory solution as '1: Fair.' Detailed explanations will be given later together with "1.5D problem" solutions in **4.2**.

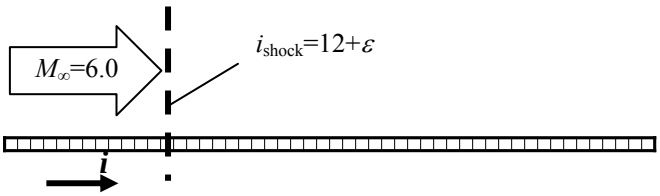

Fig. 3 Computational grid and conditions for 1D steady normal shock Test.

Fig. 4 Typical solutions of Mach number contours for 1D steady normal shock test.

4.2 1.5D (One-and-Half Dimensional) Steady Normal Shock Test

Next we will solve a steady shock that is initially aligned in one direction in a 2-D field (Fig. 5). We expected that such a computed flowfield should behave in a 1-D manner unless multidimensional instability is introduced, and thus, we called this problem a "1.5D test.[4]" This is a simplified carbuncle problem that was developed first by Quirk[3] and modified by Dumbser et al.,[31] but we used a grid that is extended farther downstream from the shock: 50×25 cells spaced evenly without any perturbation (no other kinds of perturbations are introduced either). The freestream Mach number chosen is M_∞=6.0, again. The periodical condition is imposed for the boundaries of j direction, whereas the other initial conditions and boundary conditions are the same as in the 1-D tests. The computations are conducted for 40,000 steps with CFL=0.5. If a scheme is stable for all the shock positions ε, the scheme can be labeled as 1.5D stable.

Typical solutions are shown in Fig. 6. In Figs. 4 and 6,

- '**2**' denotes a stable and symmetric solution with at least three orders of (L2-norm of) density residual reduction.
- '**1**' denotes an asymmetry and/or oscillation of the shock confined within two cells of the shock normal direction.
- '**0**' denotes an unstable solution usually associated with total breakdown of the shock ("carbuncle"). The residual stagnated at a significant value.

These points introduced in Ref. [12] will be used later in Table 2.

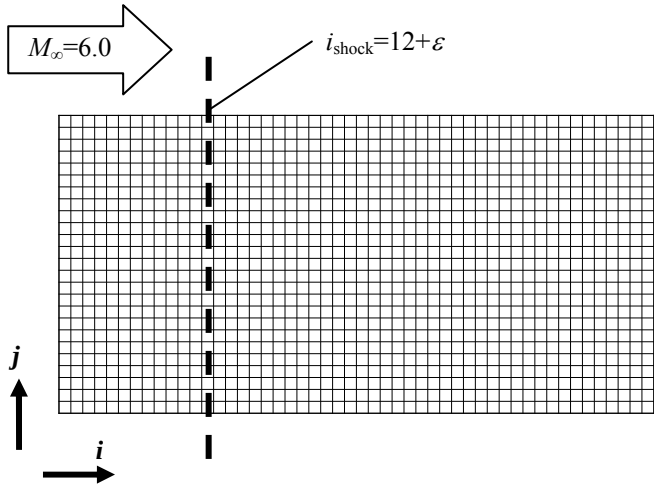

Fig. 5 Computational grid and conditions for 1.5D steady normal shock test.

(a) 2: Good (Stable)

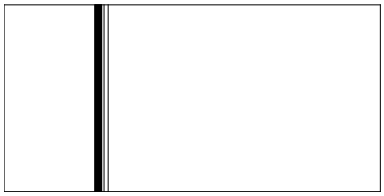

(b) 1: Fair (Oscillatory)

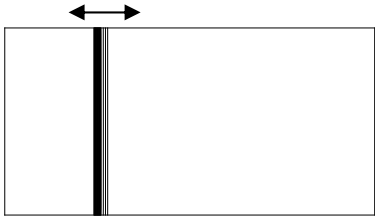

(c) 1: Fair (Asymmetry)

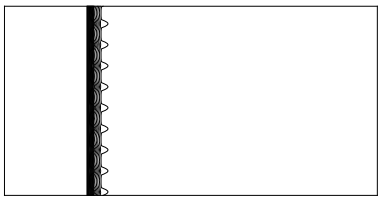

(d) 0: Poor (Instability: 'Carbuncle')

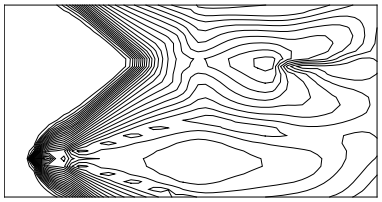

Fig. 6 Typical solutions for 1.5 dimensional steady shock test.

5 ROLE OF INTERFACIAL SPEED OF SOUND

In the present study, SLAU and AUSM+ of AUSM-family fluxes with different $c_{1/2}$ definitions are tested through the 1D and 1.5D numerical experiments. A selection of computations is summarized in Table 2. The results of Roe flux[24] are also shown for reference. Total points in terms of shock stability/robustness of each scheme are given in the rightmost column (in 40 points maximum).

Schemes and $c_{1/2}$ definitions	Test Problem	ε=0.0	0.1	0.2	0.3	0.4	0.5	0.6	0.7	0.8	0.9	**Total**
SLAU (original) [$c_{1/2}$= 0.5(c_L+c_R)]	1D	**2**	**2**	**2**	**2**	**2**	**2**	**2**	**2**	**2**	**2**	**33**
	1.5D	1	**2**	**2**	**2**	1	1	1	1	1	1	
SLAU [$c_{1/2}$=min(c_L~,c_R~)]	1D	**2**	**2**	**2**	**2**	**2**	**2**	**2**	**2**	**2**	**2**	**35**
	1.5D	**2**	**2**	**2**	1	1	1	1	1	**2**	**2**	
AUSM+ [$c_{1/2}$= 0.5(c_L+c_R)]	1D	**2**	**2**	**2**	**2**	1	1	**2**	**2**	**2**	**2**	**32**
	1.5D	**2**	**2**	**2**	**2**	1	1	1	1	1	1	
AUSM+ (original) [$c_{1/2}$=min(c_L~,c_R~)]	1D	**2**	**2**	**2**	**2**	1	1	1	**2**	**2**	**2**	**33**
	1.5D	**2**	**2**	**2**	**2**	1	1	1	1	**2**	**2**	
AUSM+ [$c_{1/2}$= *RoeAvg*(c_L,c_R)]	1D	**2**	**2**	**2**	**2**	1	1	**2**	**2**	**2**	**2**	**33**
	1.5D	**2**	**2**	**2**	**2**	1	1	1	1	1	**2**	
Roe [$c_{1/2}$= *RoeAvg*(c_L,c_R)]	1D	1	**2**	**2**	**2**	**2**	**2**	**2**	1	1	1	**22**
	1.5D	0	**2**	**2**	**2**	0	0	0	0	0	0	

Table 2 1D and 1.5D tests for schemes with various $c_{1/2}$ definitions (ε: shock location parameter[4]; the initial shock is imposed exactly on a cell-interface when ε=0.0, and at the cell-center when ε=0.5.)

The following features are noteworthy from Table 2:

- SLAU and AUSM+ both are more robust against shock anomalies than Roe flux.
- SLAU is 1D stable for all the possible shock locations ε.
- When $c_{1/2}$ is changed from arithmetic average to that of AUSM+ in which critical speed of sound is used, SLAU shows better performances in 1.5D test while retaining 1D stability. This choice is the best (total points: 35) among all the other combinations of $c_{1/2}$ and flux functions shown here.
- AUSM+, on the other hand, shows no remarkable improvements of robustness against the shock with the choice of $c_{1/2}$. For example, by changing $c_{1/2}$ from its original form to arithmetic or Roe average, its 1D stability is enhanced but the multi-dimensional stability/robustness pays the cost (this trend is consistent with original Roe and its more dissipative version, entropy-fixed Roe,[32] as shown in Ref. [4]). Consequently, overall rating for AUSM+ flux (total points: 33) is almost unaffected.

In summary, the choice of $c_{1/2}$ influences response of flux functions to the captured shock. Particularly, SLAU with $c_{1/2}$ of AUSM+ default, Eq. (5f), showed improvement of the shock stability/robustness, whereas changes of $c_{1/2}$ yielded little effect on AUSM+ flux. This difference between SLAU and AUSM+ fluxes seems to stem from the fact that SLAU has numerical dissipation term having $c_{1/2}$ (the third term of Eq. (4g)) which is absent in AUSM+. Remember that this term controls amount of dissipation. With modification of $c_{1/2}$ of SLAU from arithmetic average to the AUSM+ form, its magnitude is reduced as stated earlier (Fig. 2). From Eqs. (4g)-(4i) one can easily trace that this reduction of $c_{1/2}$ led to more dissipation in the numerical dissipation term. Thus, it is said that more proper amount of dissipation is fed into the SLAU flux by the current modification. Based on these findings, we will consider further improvement of the SLAU scheme in the next section.

6 SLAU2: IMPROVEMENT OF SLAU IN DISSIPATION TERM

6.1 Derivation of SLAU2

For clarity, Eqs. (4g)-(4i) are rewritten as follows:

Pressure term in SLAU:

$$\tilde{p} = \frac{p_L + p_R}{2} + \frac{f_{pL}^{+} - f_{pR}^{-}}{2}(p_L - p_R) + \left(1 - \left(1 - \hat{M}\right)^2\right)\left(f_{pL}^{+} + f_{pR}^{-} - 1\right)\frac{p_L + p_R}{2} \tag{8a}$$

$$\hat{M} = \min\left(1.0, \frac{1}{c_{1/2}}\sqrt{\frac{u_L^{\,2} + v_L^{\,2} + u_R^{\,2} + v_R^{\,2}}{2}}\right) \tag{8b}$$

According to this equation, at supersonic (M>1) the first parenthesis of the dissipation term, the third term of Eq. (8a), reduces to unity. In other words, the numerical dissipation introduced from this term is constant regardless of Mach number at a supersonic speed.

Then, we considered modifying this term so that the dissipation is proportional to the Mach number as follows:

$$\tilde{p} = \frac{p_L + p_R}{2} + \frac{f_{pL}^{+} - f_{pR}^{-}}{2}(p_L - p_R) + \frac{1}{c_{1/2}}\sqrt{\frac{u_L^{\,2} + v_L^{\,2} + u_R^{\,2} + v_R^{\,2}}{2}}\left(f_{pL}^{+} + f_{pR}^{-} - 1\right)\frac{p_L + p_R}{2} \tag{9}$$

Considering possible extension to real fluids,[28] the above expression is improved further.

Pressure term in SLAU2:

$$\tilde{p} = \frac{p_L + p_R}{2} + \frac{f_{pL}^{+} - f_{pR}^{-}}{2}(p_L - p_R) + \sqrt{\frac{u_L^{\,2} + v_L^{\,2} + u_R^{\,2} + v_R^{\,2}}{2}}\left(f_{pL}^{+} + f_{pR}^{-} - 1\right)\bar{\rho}c_{1/2} \tag{10}$$

This modified flux is named “SLAU2.”

6.2 Numerical Results

The newly developed scheme “SLAU2” is tested for several cases.

6.2.1. 1D and 1.5D Steady Normal Shock Tests

The first set of tests is the 1D and 1.5D steady normal shock problems. The results are summarized in Table 3.

Schemes and $c_{1/2}$ definitions	Test Problem	ε=0.0	0.1	0.2	0.3	0.4	0.5	0.6	0.7	0.8	0.9	**Total**
SLAU2 [$c_{1/2}$= 0.5(c_L+c_R)]	1D	**2**	**2**	**2**	**2**	**2**	**2**	**2**	**2**	**2**	**2**	**40**
	1.5D	**2**	**2**	**2**	**2**	**2**	**2**	**2**	**2**	**2**	**2**	
SLAU2 [$c_{1/2}$=min(c_L~,c_R~)]	1D	**2**	**2**	**2**	**2**	**2**	**2**	**2**	**2**	**2**	**2**	**40**
	1.5D	**2**	**2**	**2**	**2**	**2**	**2**	**2**	**2**	**2**	**2**	

Table 3 1D and 1.5D tests for SLAU2 flux with various $c_{1/2}$ definitions (ε: shock location parameter[4]; the initial shock is imposed exactly on a cell-interface when ε=0.0, and at the cell-center when ε=0.5.)

SLAU2 demonstrates an excellent performance against the shock anomalies regardless of the choice of $c_{1/2}$ (our experience tells that the version of $c_{1/2}$=min(c_L~,c_R~) is more robust than that of the arithmetic average, though). By adding more numerical dissipation to the flux for M>1, the improved scheme showed universal robustness (both 1D and 1.5D stabilities) against the shock. Nevertheless, we stress here that the things are not that simple: Too much dissipation addition to the flux yields 1D stability but also multi-dimensional anomalies, as reviewed above[4] for Roe flux with entropy-fix[32] or EC-Roe flux.[33] In addition, although more dissipative schemes such as HLLE,[34] Van Leer's[25] or Hänel's[35] FVS, also marked full scores (40 points) in the same test sets,[12] they are known to be incapable of capturing a contact discontinuity or a boundary-layer. Therefore, it is extremely hard to establish a scheme which is "properly dissipative" for both shock and contact discontinuities. Thus, the present scheme "SLAU2" will be tested in a boundary-layer resolution problem later in **6.2.5**.

Furthermore, similar modifications could be made for other AUSM-family fluxes having a numerical dissipation term with $c_{1/2}$ in the pressure flux, such as AUSM$^+$-up[22], but not for others, such as AUSM+ or SHUS which has $c_{1/2}$ only in the mass flux term.

6.2.2. Oblique Shock over Flat Plate with Incidence

A hypersonic flow with an oblique shock around a thin plate at M_∞=5.0 with α=5º was computed by the spatially second order code. The results are summarized in Fig. 7. Oscillations in space behind the shocks were observed in the results of SLAU and AUSM+. These wiggles, often reported for these fluxes,[12, 36] were due to lack of numerical expression for internal structure of the shock,[4, 14, 15, 16] especially where the shock jumps from one mesh line to another. In SLAU2, on the other hand, the emergence of these wiggles was successfully suppressed by proper amount of numerical dissipation addition near the shock.

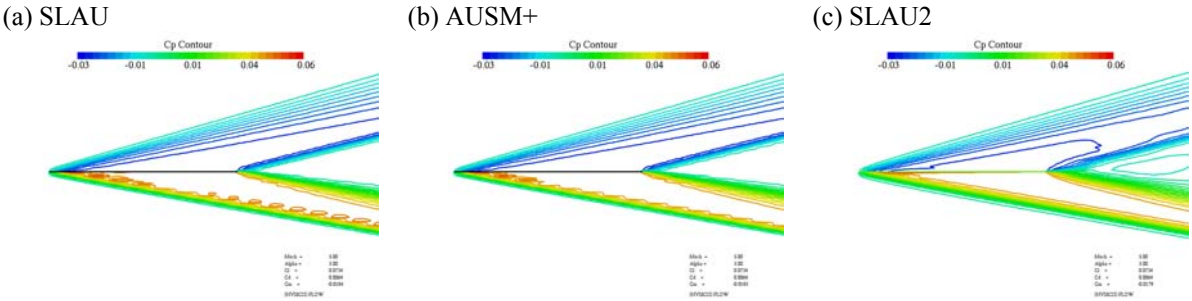

Fig. 7 Pressure contours around thin plate at M_∞=5.0, α=5 degree.

6.2.3. Low Speed Flow around NACA0012 Airfoil

It is known that at low speeds, say M<0.1, preconditioning should be used on the time-derivative and the numerical dissipation terms both.[20, 37, 38] Specifically, the latter is necessary to obtain physical solutions, whereas the former is recommended to accelerate convergence.

In this example, an inviscid flow of M_∞=0.01 around NACA0012 airfoil with no angle-of-attack[20] is calculated by using SLAU2 coupled with preconditioned LU-SGS (pLU-SGS). The code attains second order accuracy in space by Green-Gauss formula[39]. The computation was conducted for 2,000 steps with CFL=20. The result is shown in Fig. 8. For comparison, SLAU with pLU-SGS and Roe with (unpreconditioned) LU-SGS cases are also shown.

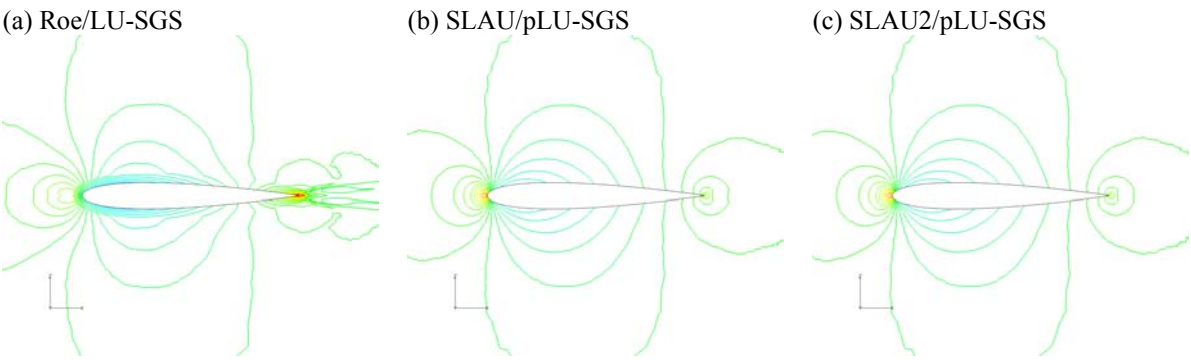

Fig. 8 Pressure contours around NACA0012 airfoil at M_∞=0.01, α=0 degree.

It is clearly seen from those figures that the SLAU2, as the original SLAU, produced a physically correct pressure profiles, whereas the Roe flux failed.

From D'Alemdert's paradox an object in an inviscid subsonic flow should have no aerodynamic drag. Thus, the drag coefficient C_D is a good measure of numerical errors introduced by the computational method used. The computed C_D showed the following values: Roe/LU-SGS (0.0720), SLAU/pLU-SGS (0.0037), and SLAU2/pLU-SGS (0.0032). SLAU2 as well as SLAU showed much smaller errors than the Roe flux.

6.2.4. Transonic Flow around NACA0012 Airfoil with Angle-of-Attack

M_∞=0.85, α=1.25º, inviscid flow around NACA0012 is computed. This example is widely used to see how fluxes and/or limiters work at a shock formed in the leeward of

the airfoil.[40, 41] Green-Gauss formula is again used for spatial reconstruction but this time coupled with Venkatakrishnan's limiter[40] with Wang's correction (ε'=0.05).[42]

The results are shown in Fig. 9. SLAU and SLAU2 are indistinguishable from the C_p graph of Fig. 9 (b), both capturing the leeward shock (x/L≈0.6; L is the chord length) without any unphysical oscillations; the Roe solution is similar to SLAU and SLAU2; AUSM+, however, showed slight spurious over/undershoots at the shock.

(a) Mach number contours (SLAU2), from black (low) to white (high)

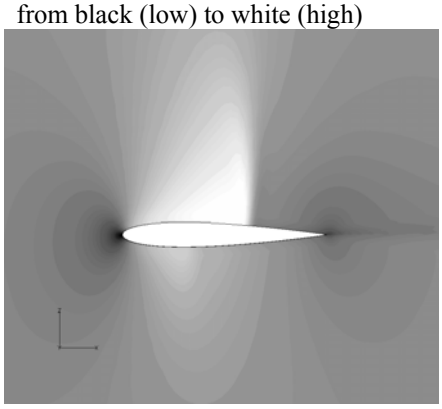

(b) Pressure profiles

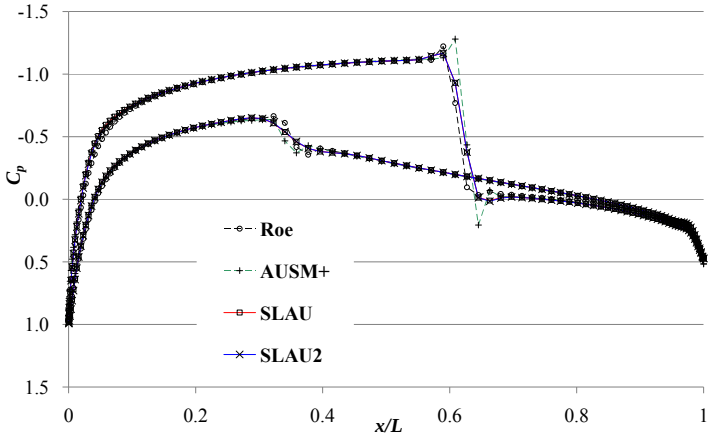

Fig. 9 Mach number contours and pressure profiles around NACA0012 airfoil at M_∞=0.85, α=1.25 degree.

6.2.5. Boundary-Layer over Flat Plate

As in Ref. [43], a M_∞=0.2 flow over a flat plate is solved by second-order Navier-Stokes code using different flux functions along with MUSCL without a limiter and second-order Runge-Kutta (Fig. 10). The computation was carried out for 50,000 time steps with CFL = 0.5 for each case. In most cases the density residual dropped at least three orders. The results showed that SLAU2 reproduced Blasius' analytical velocity profile as well as SLAU or Roe, whereas HLLE, one of notoriously dissipative solvers, did not.

Therefore, SLAU2 is considered to be "properly dissipative," because most of the other flux functions failed in either of 1D or 1.5D test, and the rare exceptions are only from the two major groups[12]: One consists of very dissipative fluxes such as HLLE,[34] Van Leer's[25] and Hänel's[35] FVSes; The other has hybrid fluxes such as AUSMDV (Shock-Fix)[44] and Rotated-RHLL,[43] which sometimes encounters difficulties in its hybridization mechanism and introduces complexity in the code. SLAU2 is the first flux which is free from any of those restrictions, i.e., free from shock anomalies, too much dissipation, or hybrid mechanisms between more than one fluxes.

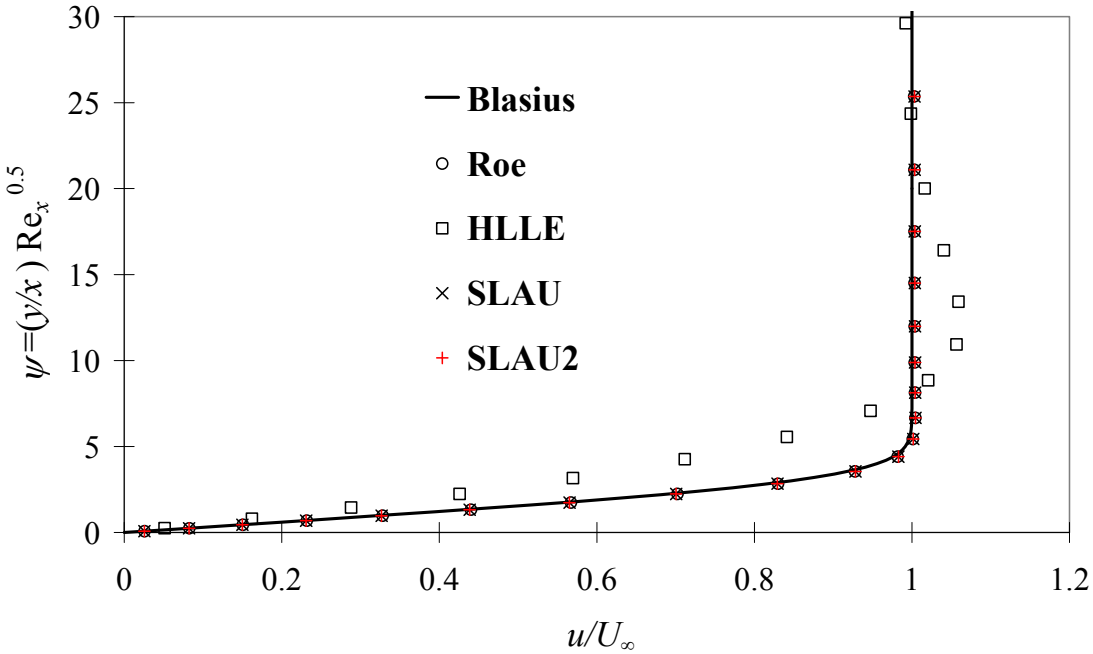

Fig. 10 Velocity profiles over flat plate at Re_x=2.2×10^4 for M_∞=0.2, α=0 degree.

7 CONCLUSIONS

Numerical experiments of hypersonic flows using AUSM-family flux functions have been conducted in one-dimensional (1D) and multi-dimensional (1.5D) contexts. We paid a particular attention to "(cell-)interfacial speed of sound," $c_{1/2}$, i.e., the speed of sound numerically defined at a cell-interface. The results are summarized as follows:

- The choice of $c_{1/2}$ generally influences response of flux functions to the captured shock.
- Particularly, SLAU (Simple Low-dissipation AUSM) with $c_{1/2}$ of AUSM+ default showed improvement of the shock stability/robustness.
- On the contrary, changes of $c_{1/2}$ yielded little effect on AUSM+ flux.

These findings motivated us further to investigate the behaviour of SLAU, our recently proposed scheme. Finally, we reached the present modification in which numerical dissipation term in the pressure flux was changed to be proportional to interfacial Mach number at supersonic speeds. The improved scheme, named SLAU2, showed the following features:

- Excellent robustness against the shock anomalies of both 1D and 1.5D irrelevant to $c_{1/2}$.
- Wiggles at an oblique shock that appeared for original SLAU or AUSM+ are eliminated.
- The numerical example of low speed flow (M_∞=0.01) demonstrated the comparable low-dissipation nature to the original SLAU.

- The solution was almost identical to the original SLAU for a transonic flow test case involving a normal shock.
- A boundary-layer over a flat plate is well resolved as the original SLAU or Roe fluxes.

Therefore, SLAU2 is considered to be "properly dissipative" for both shock and contact discontinuities, and also for low speed flow computations.

ACKNOWLEDGMENT

The set of 1D and 1.5D tests was studied while the first author visited University of Michigan, Ann Arbor, MI, under supervision of Prof. Philip L. Roe. Computational resources were partly provided by Prof. Yoshiaki Nakamura, Nagoya University, Japan. The unstructured grid solver "LS-Flow," used in **6.2.3** and **6.2.4**, was developed by Drs. Keiichiro Fujimoto and Kazuto Kuzuu with the authors at JEDI center, JAXA, Japan. Dr. Taku Nonomura, JAXA, Japan, gave us an interesting comment. We are grateful to all their support.

REFERENCES

[1] K.M. Peery and S.T. Imlay, Blunt-Body Flow Simulations, AIAA Paper 88-2904, 1988.

[2] M. Pandolfi and D. D'Ambrosio, Numerical Instabilities in Upwind Methods: Analysis and Cures for the "Carbuncle" Phenomenon, *J. Comput. Phys.,* **166**, pp.271-301 (2001).

[3] J.J. Quirk, A Contribution to the Great Riemann Solver Debate, *Int. J. Numer. Methods in Fluids*, **18**, pp.555-574 (1994).

[4] K. Kitamura, P. Roe, and F. Ismail, Evaluation of Euler Fluxes for Hypersonic Flow Computations, *AIAA J.*, **47**, pp.44-53 (2009).

[5] P. Gnoffo, G. Buck, J. Moss, E. Nielsen, K. Berger, and W.T. Jones, Aerothermodynamic Analyses of Towed Ballutes, AIAA Paper 2006-3771, 2006.

[6] K. Xu and Z. Li, Dissipative Mechanism in Godunov-type Schemes, *Int. J. Numer. Methods in Fluids*, **37**, pp.1-22 (2001).

[7] M.S. Liou, Mass Flux Schemes and Connection to Shock Instability, *J. Comput. Phys.*, **160**, pp.623–648 (2000).

[8] J.-Ch. Robinet, J. Gressier, G. Casalis, and J.-M. Moschetta, Shock Wave Instability and the Carbuncle Phenomenon: Same Intrinsic Origin?, *J. Fluid Mech.*, **417**, pp. 237-263 (2000).

[9] J.F. Coulombel, S. Benzoni-Gavage, and D. Serre, Note on a Paper by Robinet, Gressier, Casalis & Moschetta, *J. Fluid Mech.*, **469**, pp. 401-405 (2002).

[10] V. Elling, The Carbuncle Phenomenon is Incurable, *Acta Mathematica Scientia*, **29B**, pp.1647-1656 (2009).

[11] M.V.C. Ramalho and J.L.F. Azevedo, A Possible Mechanism for the Appearance of the Carbuncle Phenomenon in Aerodynamic Simulations, AIAA Paper 2010-872, 2010.

[12] K. Kitamura, E. Shima, Y. Nakamura, and P.L. Roe, Evaluation of Euler Fluxes for Hypersonic Heating Computations, *AIAA J.*, **48**, pp.763-776 (2010).

[13] P. Roe, Vorticity Capturing, AIAA Paper 2001-2523, 2001.

[14] T.J. Barth, Some Notes on Shock-Resolving Flux Functions Part 1: Stationary Characteristics, NASA TM-101087 (1989).

[15] P.L. Roe, Fluctuations and Signals—A Framework for Numerical Evolution Problems, Numerical Methods for Fluid Dynamics, edited by K. W. Morton, and M. J. Baines, Academic Press, New York, 1982, pp. 219–257.

[16] Y. Chauvat, J.M. Moschetta, and J. Gressier, Shock Wave Numerical Structure and the Carbuncle Phenomenon, *Int. J. Numer. Methods in Fluids*, **47**, pp.903–909 (2005).

[17] R. Sanders, E. Morano, and $\mathcal{M}\swarrow\mathcal{C}\swarrow$ Druguet‡⇔ Multidimensional Dissipation for Upwind Schemes: Stability and Applications to Gas Dynamics, *J. Comput. Phys.*, **145**, pp.511-537 (1998).

[18] R. Paciorri and A. Bonfiglioli, A Shock-Fitting Technique for 2D Unstructured Grids, *Computers & Fluids*, **38**, pp.715-726 (2009).

[19] E. Shima and K. Kitamura, On New Simple Low-Dissipation Scheme of AUSM-Family for All Speeds, AIAA Paper 2009-136, 2009.

[20] K. Kitamura, K. Fujimoto, E. Shima, and Z.J. Wang, Performance of Low-Dissipation Euler Fluxes and Preconditioned Implicit Schemes in Low Speeds, AIAA Paper 2010-1272, 2010.

[21] M.S. Liou, A Sequel to AUSM: AUSM+, *J. Comput. Phys.*, **129**, pp.364–382 (1996).

[22] M.S. Liou, A Sequel to AUSM, Part II: AUSM+-up for all speeds, *J. Comput. Phys.*, **214**, pp.137-170 (2006).

[23] M.S. Liou and J.R. Edwards, Numerical Speed of Sound and Its Application to Schemes for All Speeds, NASA-TM-209286, 1989; AIAA Paper 99-3268-CP, 1989.

[24] P.L. Roe, Approximate Riemann Solvers, Parameter Vectors, and Difference Schemes, *J. Comput. Phys.*, **43**, pp.357–372 (1981).

[25] B. Van Leer, Flux-Vector Splitting for the Euler Equations, *Lecture Notes in Physics*, **170**, pp.507–512 (1982).

[26] B. Van Leer, Towards the Ultimate Conservative Difference Scheme. V. A Second-Order Sequel to Godunov's Method, *J. Comput. Phys.*, **32**, pp.101-136 (1979).

[27] G.D. Van Albada, B. Van Leer, and W.W. Roberts, Jr., A Comparative Study of Computational Methods in Cosmic Gas Dynamics, *Astron. Astrophys.*, **108**, pp.76-84 (1982).

[28] J.R. Edwards, Towards Unified CFD Simulation of Real Fluid Flows, AIAA Paper 2001-2524, 2001.

[29] E. Shima, T. Nagata, and A. Ochi, Analysis of high lift configuration using unstructured overset mesh and improved SHUS, Proceedings of 20th CFD symposium of JSFM, 2006 (in Japanese).

[30] E. Shima and K. Kitamura, On AUSM-Family Scheme for All Speeds with Shock Detection for Carbuncle-Fix, AIAA Paper 2009-3544, 2009.

[31] M. Dumbser, J.M. Moschetta, and J. Gressier, A Matrix Stability Analysis of the Carbuncle Phenomenon, *J. Comput. Phys.*, **197**, pp.647-670 (2004).

[32] A. Harten, High Resolution Schemes for Hyperbolic Conservation Laws, *J. Comput. Phys.*, **49**, pp.357-393 (1983).

[33] F. Ismail and P.L. Roe, Affordable, Entropy-Consistent Euler Flux Functions II: Entropy Production at Shocks, *J. Comput. Phys.*, **228**, pp.5410-5436 (2009).

[34] B. Einfeldt, On Godunov-Type Methods for Gas Dynamics, *SIAM Journal on Numerical Analysis*, **25**, pp.294-318 (1998).

[35] D. Hänel, R. Schwane, and G. Seider, On the Accuracy of Upwind Schemes for the Solution of the Navier-Stokes Equations, AIAA Paper 87-1105, 1987.

[36] K.H. Kim, C. Kim, and O.H. Rho, Methods for the Accurate Computations of Hypersonic Flows I. AUSMPW+ Scheme, *J. Comput. Phys.*, **174**, pp.38-80 (2001).

[37] J.M. Weiss and W.A. Smith, Preconditioning Applied to Variable and Constant Density Flows, *AIAA J.*, **33**, pp.2050–2057 (1995).

[38] E. Turkel, Preconditioning Technique in Computational Fluid Dynamics, *Annu. Rev. Fluid Mech.*, **31**, pp.385-416 (1999).

[39] D.J. Mavriplis, Revisiting the Least-Squares Procedure for Gradient Reconstruction on Unstructured Meshes, AIAA Paper 2003-3986, 2003.

[40] V. Venkatakrishnan, Convergence to Steady State Solutions of the Euler Equations on Unstructured Grids with Limiters, *J. Comput. Phys.*, **118**, pp.120-130 (1995).

[41] J.S. Park, S.H. Yoon, and C. Kim, Multi-dimensional Limiting Process for Hyperbolic Conservation Laws on Unstructured Grids, *J. Comput. Phys.*, **229**, pp.788-812 (2010).

[42] Z.J. Wang, A Fast Nested Multi-Grid Viscous Flow Solver for Adaptive Cartesian/Quad Grids, *Int. J. Numer. Meth. Fluids*, **33**, pp.657-680 (2000).

[43] H. Nishikawa and K. Kitamura, Very Simple, Carbuncle-Free, Boundary-Layer Resolving, Rotated-Hybrid Riemann Solvers, *J. Comput. Phys.*, **227**, pp.2560-2581 (2008).

[44] Y. Wada and M.S. Liou, An Accurate and Robust Flux Splitting Scheme for Shock and Contact Discontinuities, *SIAM J. Sci. Comput.*, **18**, pp.633-657 (1997).